A Vision-Aided Approach to Perching a Bioinspired Unmanned Aerial Vehicle

Cai Luo, *Senior Member, IEEE*, Leijian Yu, and Peng Ren, *Senior Member, IEEE*

***Abstract*—This paper presents the implementation of a machine learning approach for replicating highly adaptive avian perching behavior. With full consideration of both the configuration of flying vehicles and perching principles, a bioinspired aerial robot comprising one flight subsystem and one perching subsystem is designed. Based on the real-time landing speed and attitude, a novel type of soft grasping mechanism for dexterous perching is proposed to provide adhesive force and absorb impact force. During the critical perching phase, the dynamics of the perching actuator change with the touchdown conditions and the type of perching target. A hybrid automation of a time-to-contact theory-based attitude controller and a robust self-localization system are utilized to regulate the desired perching maneuvers. The experimental results are provided to attest to the effectiveness of the proposed perching method.**

***Index Terms*—Bioinspired, machine learning, unmanned aerial vehicle (UAV).**

NOMENCLATURE

f_T	Claw impact force.
f_N	Static friction.
F_{servo}	Pulley tension force.
τ_{motor}	Total pulley torque generated by motor.
R	Pulley radius.
R_1	Upper joints rotate radius.
R_2	Lower joints rotate radius.
l_1	Upper phalange length.
l_2	Lower phalange length.
C_i	Material constant.
λ	Axial principle stretch ration.
$G(t)$	Action gap.
$\dot{G}(t)$	Closure rate of action-gap.
D	Distance gap to the target.
$d(t)$	Straight distance to the docking point in terms of time.
V_s	Current speed.
P	3-D Position vector.
α	Angle related to the perching target.
diag	Diagonal matrix.
g	Gravity.
m_c	Mass of the claw.
m_u	Mass of the UAV.
V_c	Claw speed related to the target.
V_u	UAV speed related to the target.

Manuscript received June 27, 2017; revised September 17, 2017; accepted October 6, 2017. Date of publication October 19, 2017; date of current version January 16, 2018. This work was supported in part by the National Natural Science Foundation of China under Grant 61701541 and Grant 61671481, in part by the Shandong Provincial Natural Science Foundation, China, under Grant ZR2017QF003, and in part by the Qingdao Applied Fundamental Research under Grant 16-5-1-11-jch. *(Corresponding author: Cai Luo and Peng Ren.)*

C. Luo is with the College of Mechanical and Electronic Engineering and Oil Industry Training Center, China University of Petroleum (East China), Qingdao 266580, China (e-mail: tsai.lo.95@gmail.com).

L. Yu and P. Ren are with the College of Information and Control Engineering, China University of Petroleum (East China), Qingdao 266580, China (e-mail: yuleijian@s.upc.edu.cn; pengren@upc.edu.cn).

Color versions of one or more of the figures in this paper are available online at http://ieeexplore.ieee.org.

Digital Object Identifier 10.1109/TIE.2017.2764849

I. INTRODUCTION

OVER the past few years, a multitude of efforts has been made to utilize unmanned aerial vehicles (UAVs) for deployment in unstructured and dynamic environments. Examples of applications can be gathered from a number of recent journals, magazines, and news headlines, with topics ranging from aerial surveillance and security to the inspection of complex environments [1], [2]. Within the family of UAVs, vertical take off and landing (VTOL) rotor craft have gain particular interest owing to their capability to hover in flight, small size and agility [3]. Meanwhile, it is a common assumption that landing ground is always available for UAVs during a mission. However, this is an unrealistic condition in search, surveillance, and rescue tasks. Outside laboratories, UAVs may quite easily encounter weather that is too rough to continue their missions when there is no UAV airport nearby [4], severely limiting the usable conditions of UAVs [5], [6].

In nature, avians exhibit a perching landing mode for energy economy, and this mode is typically used for looking, resting, and hiding from natural enemy [7]. As a fast landing behavior, perching refers to a high-speed surface impact, the provision of effective friction, and the localization of a precise landing area. Cory and Tedrake initially analyzed and designed a fixed-wing UAV perching experiment and suggested that proper angles-of-attack are essential for landing on a perch [8]. Afterward, different bioinspired mechanical models were demonstrated to attest to this assertion [9]–[11]. For example, the Biomimetics and Dexterous Manipulation Lab at Stanford University proposed a pitch-up landing procedure consisting of elevator up, plane nose up, and zero-speed touchdown on a wall [10]. Within this architecture, the possibility of perching on vertical surfaces via a combination of impact force absorption and the release of adhesion force was numerically confirmed with reasonable

aerodynamic assumptions. Other perching approaches include a passive claw-like gripper [12]–[14], dry/wet/electrostatic adhesives [15]–[17], and spines that can penetrate into a soft landing substrate [18]. Accordingly, the authors concluded that perching could be an energy-saving behavior. By virtue of this ability, avians may occupy a high vantage point for an extended period of time, which is crucial in hunting, hiding, and mating.

Nowadays, in most safety, security, and rescue missions, UAVs keep flying in the air. With the demand to provide inconspicuous closer inspection in unstructured environments [18], this paper focuses on the design and implementation of a novel UAV system based on our previous work on bioinspired UAV landing [19]. The new platform uses a time-to-contact theory-based attitude controller working with a self-localization algorithm, which enables a VTOL, UAV to autonomously land on a tree branch-like surface in an urban environment.

The main contribution of this paper consists of the explicit design of biomimetic perching actuators via hybrid deposition manufacturing, robust perching maneuver models, a real-time machine learning approach that can run on an embedded development board to achieve the precise landing of a VTOL UAV and the consequent experimental appraisal of the presented platform. We present the dynamics of a VTOL UAV landing on a tree branch-like surface and construct a hybrid self-localization controller along with appropriate reference trajectories. The performance and robustness of the proposed perching actuators guarantee that the UAV does not fall down and that the impact force is sufficiently absorbed so that the UAV's fuselage does not rip apart [20].

This paper is organized as follows. Section II introduces the biomimetic VTOL UAV prototype and hardware configuration. In Section III, we present the dynamical and FEM model of the UAV gripper. The perching algorithm, machine learning approach, and control strategy are discussed in Section IV. The experimental setup used to evaluate the proposed architecture and related results are detailed in Section V. Finally, the conclusion and future work are presented in Section VI.

II. UAV Prototype and Hardware

The VTOL UAV considered in this paper is a quadrotor helicopter equipped with a soft bioinspired gripper with perch capabilities.

As shown in Fig. 1, the gripper mechanism is mounted under the VTOL UAV to facilitate branch perching. The requirements for gripper engagement include

1) the possible touchdown velocities and attitude of the UAV as it approaches the target;
2) the mechanical properties of the gripper that absorbs the landing impact force and prevents rebound.

Once the perching target is detected, the landing procedure will be visual guided using close-loop control, with enough maneuverability to keep the VTOL UAV stable and to prevent sensitivity to turbulent flow. The general sequence is

i) flying above the landing area and searching for the perching target;

Fig. 1. Three-dimensional schematic of the developed UAV.

ii) decreasing the thrust output and lowering the altitude by the perch control strategy, which will be discussed in Section IV;
iii) maintaining the approach attitude and velocity to position the UAV for perching;
iv) gripper actively wrapping around the perching target to obtain an enclosure grasp and to absorb the impact force with a soft joint.

III. Gripper Modeling

A. Analytical Modeling

The potential impact energy of the coupled perching system is determined by

$$U = m_c g \bullet V_c + m_u g \bullet V_u. \tag{1}$$

Following the observation during the perching tests that tumbling was the main cause affecting control performance, the docking control goal was formulated to minimize the perching speed in the vertical direction to decrease the force of the impact.

We then demonstrate the concept of our gripper kinematic equations and the process of manufacturing the gripper. The claw mechanisms are designed to fulfill the following requirements:

1) The joints can extend the contact time to absorb the impact energy.
2) The claw can perform a variety of grasps. Specifically, the phalanges perform a wrapping grasp around irregular object surfaces and a variety of object sizes [9].
3) The mechanism should have an impact force protection that prevents structural damage when the landing speed exceeds the ideal perching velocity [21].
4) The grip force between the mechanism and the perching target should help manage horizontal turbulence [13].

The under-actuated gripper consists of two identical claws with a distance of $2b$ for base length. Each claw consists of two rigid straight phalanges. The phalanges are connected through a soft flexure designed joint to allow a small twisting in response

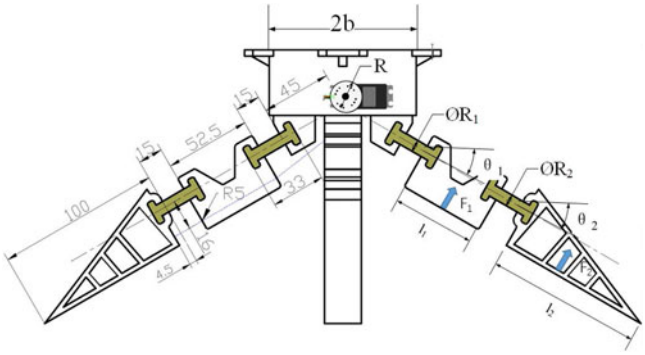

Fig. 2. Technical drawing of the proposed gripper.

to unforeseen branch shapes. The soft perching mechanism is described through geometrically constant parameters, as shown in Fig. 2. Once the gripper is fully in contact with the target, the gripper and target are rigidly assembled into a constrained linkage.

When the VTOL UAV perches on the target, the claw achieves a successful enveloping grasp in which the VTOL UAV body is physically constrained by the claw actuator. For this perch scenario, the applied claw impact force to the cylinder is equal to the static friction, and therefore, $f_T = \mu_k f_N$.

The pulley tension force on each claw's tendon F_{servo} is calculated as [22]

$$F_{\text{servo}} = \frac{1}{4}\frac{\tau_{\text{motor}}}{R} \tag{2}$$

where τ_{motor} denotes the total pulley torque generated by the motor and R denotes the pulley radius. This behavior results in the actuator force being evenly distributed to the four fingers.

$$F_1 = \frac{2}{l_1}R_1 F_{\text{servo}} - \frac{2(l_1 cos\theta_2 + \frac{l_2}{2})}{l_1}F_2$$
$$F_2 = \frac{2R_2}{R_1 l_2}R_1 F_{\text{servo}} \tag{3}$$

where R_1 and R_2 represent the rotation radius of the upper and lower joints, respectively. The lengths of the upper and lower phalanges are denoted by l_1 and l_2, respectively.

The flexure joint actuators were fabricated using hyperelastic silicone rubber. The joints were modeled as Yeoh material [23], so the strain energy can be written as

$$W = \sum_{i=1}^{n} C_i (I_1 - 3)^i$$
$$I_1 = \lambda^2 + \frac{2}{\lambda} \tag{4}$$

where C_i is the material constant and λ equals the axial principle stretch ratio.

B. Finite-Element Method (FEM) Modeling

To demonstrate the structural damping properties of the soft joint, a 3-D FEM model is built and analyzed with ANSYS, which was used to simulate the perching tests. All the components of the claw were made by using the mechanical data of the

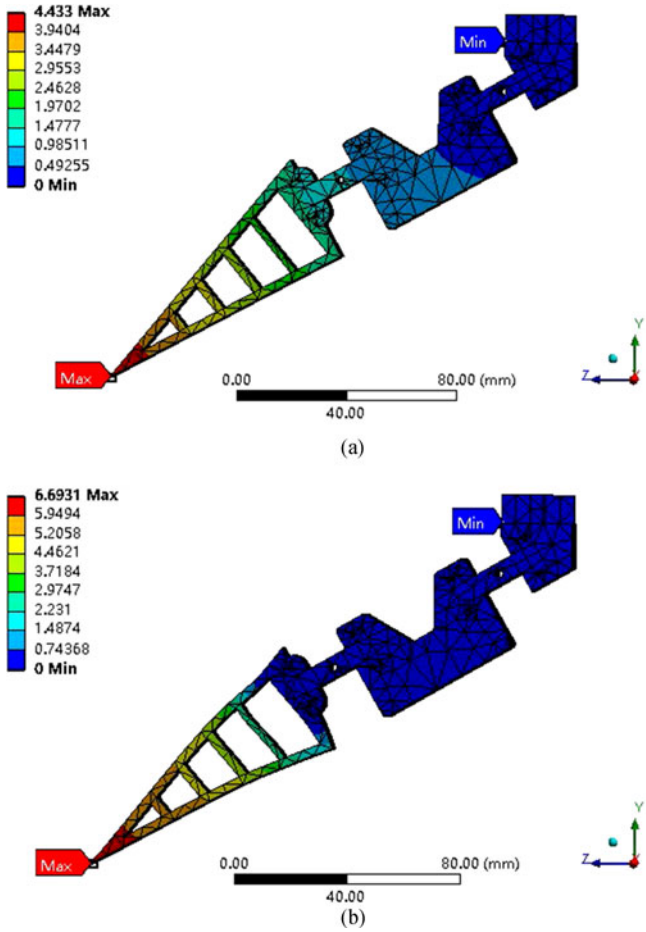

Fig. 3. Maximum displacement of the claw joints using FEM model. (a) Soft joint (silicon rubber). (b) Rigid joint (plastic).

VTOL UAV. A total of 11 193 nodes and 5248 elements were used to model the claw.

Prior to the simulations, the elastomeric materials used to fabricates the claw joints were tested by a static/dynamic universal testing machine (SGX-400-1000) at a stretch/compress rate of 300 mm/min for uniaxial material properties. For the sake of simplified discussion, the material behaviors of the elastosil and the polyethylene are modeled by Yeoh's hyperelastic incompressible algorithm [23], [24]. The strain energy for elastosil material is denoted as (4), where $C_1 = 0.11$ MPa, $C_2 = 0.02$ MPa. The numerical models of phalanges and joints were completely fixed, and 10 N (weight of the VTOL UAV) of an uniform load was applied to the inside surface of the claw in the vertical direction. For comparison, the same claw with an equal weight was simulated using the normal polylactic acid material (with a Young's Modulus 3.5 GPa, poisson's ratio of 0.36, and density of 1.25 g/cm^3).

As expected, the modeled hyperelastic joint elements introduced some impact damping support. Fig. 3 shows the FEM results. The maximum displacement of the soft joint (silicon rubber) model is 4.433 mm, and that of the rigid joint (plastic) model is 6.693 mm. Therefore, it can be said that the newly designed claw would help the VTOL UAV to withstand disturbances that may influence the approach speed.

IV. Perch Control Strategy

A. Perch Algorithm

Based on Lee's theory [25], goal-directed action is the key factor for animal approaching an object or target [26]. An action-gap is used to describe the state difference between the current situation and the goal state. In our case, the action-gap is the difference between hovering state and a hazardous surface landing/docking state. The tau (τ) of an action-gap (G) is denoted as

$$\tau(t) = \frac{G(t)}{\dot{G}(t)} \tag{5}$$

where $G(t)$ is the action-gap and $\dot{G}(t)$ denotes the closure rate of an action-gap.

Inspired by the tau-control law [27], a UAV-oriented landing control algorithm is proposed as

$$\tau_{\text{target}} = k_{ts}\tau_{\text{speed}}. \tag{6}$$

For the perching tasks, the VTOL UAV will decrease the gap distance and the velocity to zero at the same time. From the (6) above, the perching trajectory can be denoted as

$$\begin{aligned} D_{\text{target}} &= \Delta V_s^{\frac{1}{k_{ts}}} \\ \dot{D}_{\text{target}} &= \frac{\Delta}{k_{ts}} V_s^{\frac{1}{k_{ts}}-1}\dot{V}_s \\ \ddot{D}_{\text{target}} &= \frac{\Delta}{k_{ts}} V_s^{\frac{1}{k_{ts}}-2}\left(\frac{1-k_{ts}}{k_{ts}}\dot{V}_s^{\,2} + V_s\ddot{V}_s\right) \end{aligned} \tag{7}$$

where Δ is a constant defined as $\Delta = D_{\text{target}}(0)/V_s(0)^{\frac{1}{k_{ts}}}$.

The VTOL UAV does not have a long taxiing runway as do fixed-wing UAVs. This UAV requires a gentle vertical touchdown for a perching task. In this situation, the angle gap in terms of time can be denoted as

$$\theta(t) = \theta(0)\frac{D_{\text{target}}(t)^{\frac{1}{k_{D\theta}}}}{D_{\text{target}}(0)^{\frac{1}{k_{D\theta}}}}. \tag{8}$$

Combining (7) and (8), which represent the perching trajectory and angle gap, respectively, the VTOL UAV position P can be denoted as follows:

$$\begin{aligned} P(t) &= A_1P(t_d) + A_2P(0) + A_3 \\ A_1 &= \text{diag}\left(1 - \frac{d(t)\sin\alpha(t)}{d(0)\sin\alpha(0)}, 1 - \frac{d(t)\sin\alpha(t)}{d(0)\sin\alpha(0)}, 1\right) \\ A_2 &= \text{diag}\left(\frac{d(t)\sin\alpha(t)}{d(0)\sin\alpha(0)}, \frac{d(t)\sin\alpha(t)}{d(0)\sin\alpha(0)}, 0\right) \\ A_3 &= [0 \quad 0 \quad d(t)\sin\alpha(t)] \end{aligned} \tag{9}$$

where α denotes the angular related to the perching target, as shown in Fig. 4, and diag denotes a diagonal matrix.

By analyzing (7) and (9), we found that when $k_{ts} \in (0.5, 1)$, the UAV can smoothly land on the surface or can incur a small collision with the landing site without harming the structure of the platform.

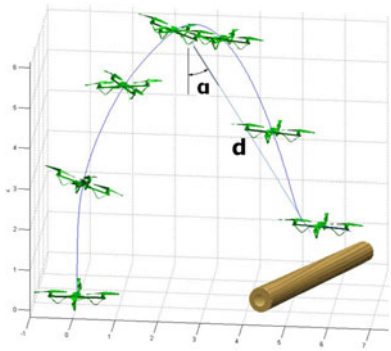

Fig. 4. Simulation of the VTOL UAV perch path.

B. Algorithm of the Vision-Aided Autonomous Perching System

In order to successfully perch on a tree branch, the VTOL UAV has to perceive where the target is and then maneuvers in order to land on the branch. Inspired by YOLO [28], we use a convolutional neural network (CNN) module [29], [30], and the network architecture is elaborated in Fig. 5. The CNN module is a feedforward model built out of successive pairs of convolutional layers, pooling layers and fully connected layers. In order to increase the perching success rate, a regression detection model to identify the perching target is trained. The input image is divided into S^*S grid cells equally, each grid cell regresses B bounding boxes that may contain the perching target, and at the same time, each grid cell predicts the probabilities of C categories of perching targets. The 2500 training frames with a size of 224 × 224 are used in our tests as training data. These data were collected over 20 different outdoor locations.

Table I elaborates on the proposed CNN layer configuration. The input three-channel image is first processed in the C_1 layer by a convolutional activation pooling operation to generate 16 feature maps with the size of 56 × 56. Similarly, the C_2 layer generates 32 feature maps with a size of 28 × 28, the C_3 layer generates 64 feature maps with a size of 14 × 14 and the C_4 layer generates 128 feature maps with a size of 7 × 7. Finally, a 4096-dimensional vector is processed to generate a 7 × 7 × 11 prediction tensor.

For evaluating the perching target dataset, we use convolutional filters with a size of 3 × 3 and a pooling receptive field with a size of 2 × 2. We use a linear activation function for the final detection layer, and all other layers use the following leaky rectified linear activations (10):

$$f(x) = \begin{cases} x, & x > 0 \\ 0.1x, & x \le 0. \end{cases} \tag{10}$$

For evaluating the suitable perching target dataset, we use $S = 7$ (square grid number), $B = 2$ (bounding box number), and $C = 1$ (class number) with respect to the perching targets. Our final prediction for a given image is encoded as a 7 × 7 × 11 tensor.

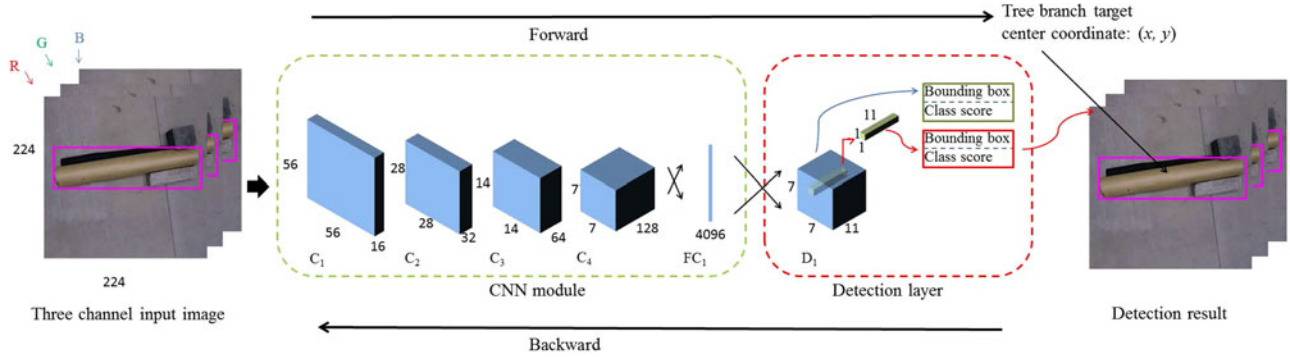

Fig. 5. Full architecture of the proposed regression-based detection model. The proposed detection model architecture consists of a CNN module and a detection layer. The input image is feed into the CNN module, and the CNN module is followed by a detection layer. After the training, the detection layer generates the prediction, which consists the bounding box information and the class probability of the detected object.

TABLE I
CANDIDATE PARAMETRIC VALUES OF AUGMENTATION PARAMETERS AND CNN HYPER-PARAMETERS FOR GRID SEARCH

C_n	Layer Configuration
C_1	Conv filter $3 \times 3 \times 16$, stride 2 Maxpooling 2×2, stride 2
C_2	Conv filter $1 \times 1 \times 8$, stride 1 Conv filter $1 \times 1 \times 32$, stride 1 Conv filter $3 \times 3 \times 32$, stride 1 Maxpooling 2×2, stride 2
C_3	Conv filter $1 \times 1 \times 16$, stride 1 Conv filter $1 \times 1 \times 64$, stride 1 Conv filter $3 \times 3 \times 64$, stride 1 Maxpooling 2×2, stride 2
C_4	Conv filter $3 \times 3 \times 128$, stride 1 Maxpooling 2×2, stride 2

C. Autonomous Perching Strategy

Algorithm 1 illustrates the perching strategy for the VTOL UAV.

Algorithm 1: Policy for Autonomous Perching.

Require: Real time image; ultrasonic distance data; air pressure data
while Height $\leq$ 3 m **do**
  Search for perching target
  if Landing area detected & Distance gap $>$ 3 cm **then**
    Tau perch control
  else if Landing target detected & Distance gap $\leq$ 3 cm **then**
    Thrust power decreases to idle speed and claw starts to close
  else
    Increase flight height
  end if
end while

The system as shown in Fig. 6 is designed to support a real-time CNN-assisted program. The on-board electronics consist of three intercommunicable levels: the aerial control unit (ACU); the operation unit (OU); and the perching unit (LU).

To save training time, the most popular device for training a deep learning model is the GPU. In this paper, we take an identical training strategy for training the proposed regression-based detection model. The inference procedure is loaded on an embedded development board after the detection model is trained on a GPU. The detection model is optimized by stochastic gradient descent [31], with gradients being back-propagated through the whole network. During the tree branch dataset training procedure, a data jittering approach, which changes the rotation, translation, and shearing of the original images, is taken to augment the dataset. Adjusting the image exposure, saturation and hue are used to further increase the training set. The detection model is trained on a laptop equipped with an NVIDIA 860M GPU and then loaded on the on-board single-board computer.

The CNN-assisted perching program is performed on the OU controller, which has an on-board computer. The state estimation and attitude control are made by the ACU flight autopilot. The ACU autopilot receives the acceleration, ascend and descend commands coming from either the on-board computer or the OU controller.

V. EXPERIMENTAL RESULTS

The performance of the proposed biomimetic UAV system is evaluated via extensively tests and has demonstrated robust and precise control of the aerial vehicle in many hazardous situation. In all flight tests, there is no prior environment information provided to the vehicle.

The characteristics of the platform are summarized as follows:

1) Flying System
   On-board processor: the processor is a DJI Manifold microcontroller board with an NVIDIA Tegra K1 CPU that can reach 2.2 GHz. The board includes four ARM-Cortex A15 cores and 192 GPU CUDA cores and weighs approximately 200 g with a size of 11 cm(width) $\times$ 11 cm(length) $\times$ 2.6 cm(height).
   Electronics controlling devices: the electronic devices include a Pixhawk flight autopilot, which has an inertial measurement unit (IMU) and four hobbywing flyfun 40A

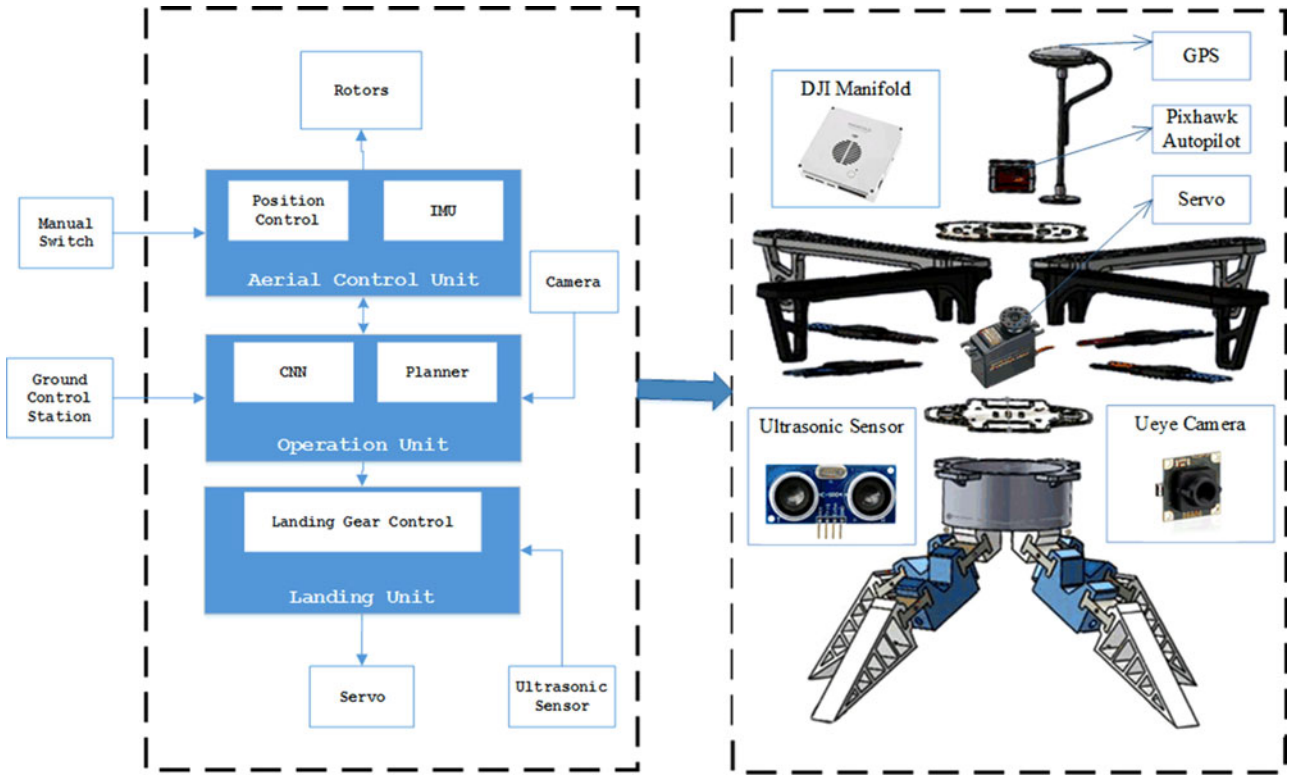

Fig. 6. Integration system of the multirotor helicopter system and the vision landing platform.

electronics speed controllers (ESC) to vary electric motor speed.

Airframe: the structure of the airframe is built using a fiber composite X-shaped frame. The main body consists of four motors, four ESCs, an IMU, and an on-board computer. Motors with 10 in propellers produce a maximum propulsion of 500 g.

Operating system (OS): the on-board OS, which is running as middleware, is the robotic OS (ROS) [32]. Each processing thread is considered as a node in the ROS, and each node communicates with others via messages transmitted through communication protocols. The UAV ROS OS also sends the essential flight data to the ground control station (GCS). The GCS is used only to display the real-time state of the UAV, to show the processing result of the vision algorithm and to prove the landing request based on the landing site quality result. For safety reasons, a human pilot can switch to manual control via the radio when the UAV performs unplanned movement.

Communication protocol and path: the Mavlink protocol forms the backbone of the communication link onboard. The IMU and the on-board processor (pxCOMex) use the Mavlink to send UAV states and flight control commands. The UAV and GCS are connected via a wireless UART since UART is more suitable for long-range data transmission.

2) Perching System

Claw controlling devices: an Arduino 32-channel servo motor controls driver board and a KST 825MG digital servo with a torque of 35 kg/cm(8.4 v) and reaction speed of 0.11 s/60°(8.4 v).

Visual devices: a USB IDS uEye LE Camera with a 58° FOV lens (UI-1221LE-M-GL, CMOS, 87.2 fps, 752 × 480, global shutter) mounted beneath the quadrupedal platform.

Perching detective device: a TELESKY HC-SR04 ultrasonic range finder. The detection range is between 2 and 450 cm with 0.3-cm accuracy.

Communication protocol: the quadrupedal and UAV are connected through a universal synchronous/asynchronous receiver/transmitter.

To evaluate the perching performance and the machine learning method, 40 real-field experiments using the bioinspired VTOL UAV were carried out in an outdoor area. The flight tests were performed on sunny and cloudy days with wind speeds below 10 m/s. At present, the bioinspired VTOL UAV has successfully achieved autonomous perching by use of our machine-learning approach, and no prior trajectory information is provided to the UAV.

During the autonomous perching tests, there are always two pilots monitoring the states of the UAV for safety reasons. One person is in charge of the GCS and monitors the real-time flight data. The other person, whose duty is to take over control of the UAV in the event of any abnormal movement, takes responsibility of the radio controller. Both pilots have the right to send the command of shutting down all the rotors immediately. The UAV is 70 cm wide from tip to tip and 28 cm high. The length of the perching gear is 22.7 cm.

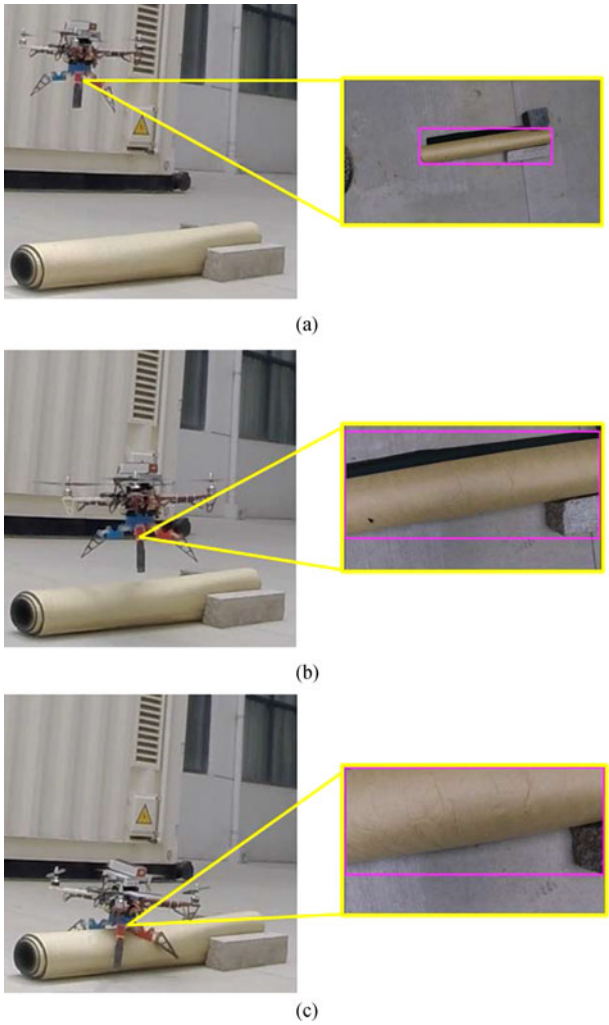

Fig. 7. Experimental snapshots of VTOL UAV perching. The camera is placed downward for the search process. (a) Take-off and start to search for the potential perching target. (b) Perching target detected and flight height decreased. (c) Thrust power decreased to idle speed and claw closed.

For the evaluation of the versatility of the UAV, we executed the autonomous perching procedure, as shown in Fig. 7, in 40 tests with different environmental conditions.

During the experiments, the UAV attempted to perch on a cylinder with different diameters ranging between 5 and 50 cm, all of which are found in typical outdoor environments.

In these 40 perching tests, the UAV is capable of landing on a cylinder with a 28 cm diameter. Fig. 8 displays the attitude estimation, roll angle, pitch angle, yaw angle, and vertical height over time in the perching process. The root mean squared error (RMSE) of the distance between the target and the quadrotor is shown in Table II, and the attitude performance error is shown in Table III. The position RMSE error is 6 cm in the horizontal plane (real docking point respect to planned perch point) and 7 cm in the vertical plane (real zero speed point height with respect to the planned zero speed point height). As demonstrated, the landing mechanism is fully capable of perching on a tree trunk with a diameter between 15 and 50 cm.

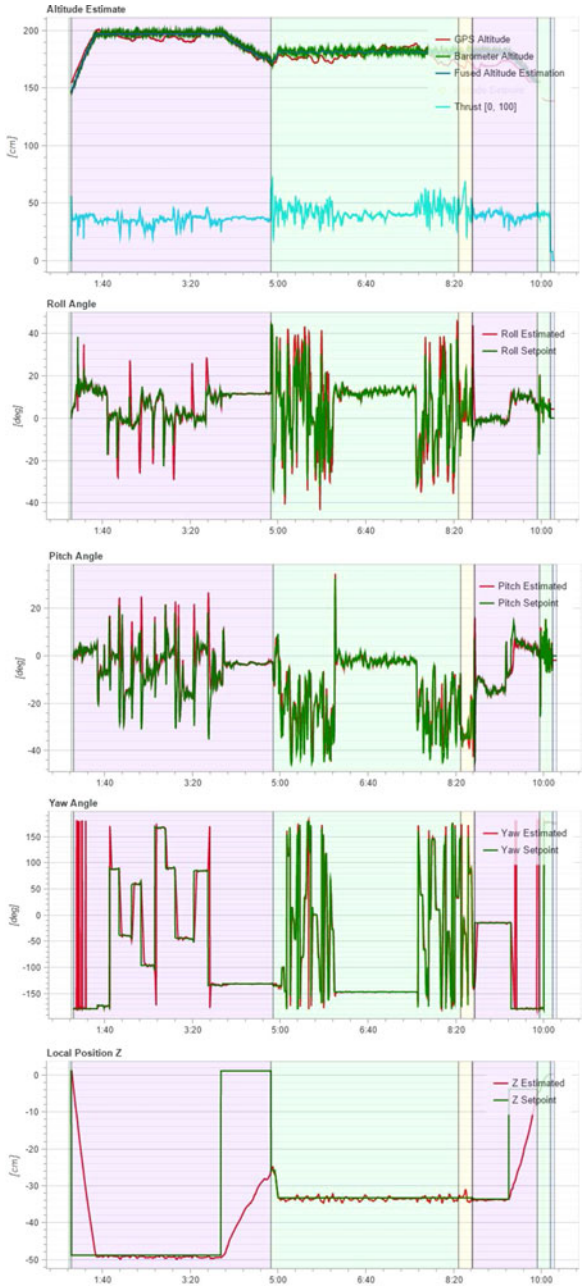

Fig. 8. Plots of the attitude estimation, roll angle, pitch angle, yaw angle, and vertical height over time in the perching.

TABLE II
PERCHING PERFORMANCE ERROR

RMSE horizontal X,Y[m]	0.067
RMSE vertical Z[m]	0.073

TABLE III
ATTITUDE PERFORMANCE ERROR

RMSE roll[°]	1.42
RMSE pitch[°]	0.32
RMSE yaw[°]	2.53

VI. Conclusion and Future Work

This paper presented a biomimetic UAV perching control through a CNN approach. First, a bio-inspired soft perching mechanism was developed, which effectively absorbed the landing impact energy. Second, a tau theory controller was developed to fulfill the smooth landing requirement. Third, a CNN-based vision guided system was designed for the VTOL UAV. All these mechanisms and control strategies work together to render the VTOL UAV system capable of smoothly and accurately perching on a variety of challenging landing surface. The effectiveness of the proposed UAV architecture has been further verified by experiments. Future work will focus on enabling the biomimetic UAV to crawl over hazardous terrain and catch a target object like a real bird to extend the usability of UAVs. Many-core processors are also good potential solutions for power efficiency.

Acknowledgment

The authors would like to thank the technicians from the Oil Industry Training Center in China University of Petroleum for the CNC manufacturing and flight testing support.

References

[1] M. Graule *et al.*, "Perching and takeoff of a robotic insect on overhangs using switchable electrostatic adhesion," *Science*, vol. 352, no. 6288, pp. 978–982, 2016.
[2] D. Floreano and R. J. Wood, "Science, technology and the future of small autonomous drones," *Nature*, vol. 521, no. 7553, pp. 460–466, 2015.
[3] X. Zhang, B. Xian, B. Zhao, and Y. Zhang, "Autonomous flight control of a nano quadrotor helicopter in a GPS-denied environment using onboard vision," *IEEE Trans. Ind. Electron.*, vol. 62, no. 10, pp. 6392–6403, Oct. 2015.
[4] B. Xiao and S. Yin, "A new disturbance attenuation control scheme for quadrotor unmanned aerial vehicles," *IEEE Trans. Ind. Informat.*, Mar. 2017.
[5] H. Liu, D. Li, Z. Zuo, and Y. Zhong, "Robust three-loop trajectory tracking control for quadrotors with multiple uncertainties," *IEEE Trans. Ind. Electron.*, vol. 63, no. 4, pp. 2263–2274, Apr. 2016.
[6] B. Zhao, B. Xian, Y. Zhang, and X. Zhang, "Nonlinear robust adaptive tracking control of a quadrotor UAV via immersion and invariance methodology," *IEEE Trans. Ind. Electron.*, vol. 62, no. 5, pp. 2891–2902, May 2015.
[7] K. Y. Ma, P. Chirarattananon, S. B. Fuller, and R. J. Wood, "Controlled flight of a biologically inspired, insect-scale robot," *Science*, vol. 340, no. 6132, pp. 603–607, 2013.
[8] R. Cory and R. Tedrake, "Experiments in fixed-wing UAV perching," in *Proc. AIAA Guid., Navig. Control Conf. Exhibit*, 2008, pp. 1–12.
[9] A. M. Dollar and R. D. Howe, "Towards grasping in unstructured environments: Grasper compliance and configuration optimization," *Adv. Robot.*, vol. 19, no. 5, pp. 523–543, 2005.
[10] A. Lussier Desbiens, A. T. Asbeck, and M. R. Cutkosky, "Landing, perching and taking off from vertical surfaces," *Int. J. Robot. Res.*, vol. 30, no. 3, pp. 355–370, 2011.
[11] L. Daler, A. Klaptocz, A. Briod, M. Sitti, and D. Floreano, "A perching mechanism for flying robots using a fibre-based adhesive," in *Proc. IEEE Int. Conf. Robot. Autom.*, 2013, pp. 4433–4438.
[12] C. E. Doyle *et al.*, "An avian-inspired passive mechanism for quadrotor perching," *IEEE/ASME Trans. Mechatronics*, vol. 18, no. 2, pp. 506–517, Apr. 2013.
[13] M. L. Burroughs, K. B. Freckleton, J. J. Abbott, and M. A. Minor, "A sarrus-based passive mechanism for rotorcraft perching," *J. Mechanisms Robot.*, vol. 8, no. 1, 2016, Art. no. 011010.
[14] E. W. Hawkes *et al.*"Dynamic surface grasping with directional adhesion," in *Proc. IEEE/RSJ Int. Conf. Intell. Robots Syst*, 2013, pp. 5487–5493.
[15] H. Stuart, S. Wang, O. Khatib, and M. R. Cutkosky, "The ocean one hands: An adaptive design for robust marine manipulation," *Int. J. Robot. Res.*, vol. 36, no. 2, pp. 150–166, 2017.
[16] F. Connolly, C. J. Walsh, and K. Bertoldi, "Automatic design of fiber-reinforced soft actuators for trajectory matching," *Proc. Nat. Acad. Sci. USA*, vol. 114, no. 1, pp. 51–56, 2017.
[17] L. U. Odhner and A. M. Dollar, "Stable, open-loop precision manipulation with underactuated hands," *Int. J. Robot. Res.*, vol. 34, pp. 134–1360, 2015.
[18] M. Kovač, J. Germann, C. Hürzeler, R. Y. Siegwart, and D. Floreano, "A perching mechanism for micro aerial vehicles," *J. Micro-Nano Mechatronics*, vol. 5, no. 3/4, pp. 77–91, 2009.
[19] C. Luo, X. Li, Y. Li, and Q. Dai, "Biomimetic design for unmanned aerial vehicle safe landing in hazardous terrain," *IEEE/ASME Trans. Mechatronics*, vol. 21, no. 1, pp. 531–541, Feb. 2016.
[20] S. Kim, C. Laschi, and B. Trimmer, "Soft robotics: A bioinspired evolution in robotics," *Trends Biotechnol.*, vol. 31, no. 5, pp. 287–294, 2013.
[21] D. M. Aukes *et al.*, "Design and testing of a selectively compliant underactuated hand," *Int. J. Robot. Res.*, vol. 33, no. 5, pp. 721–735, 2014.
[22] G. A. Kragten and J. L. Herder, "The ability of underactuated hands to grasp and hold objects," *Mechanism Mach. Theory*, vol. 45, no. 3, pp. 408–425, 2010.
[23] O. Yeoh, "Some forms of the strain energy function for rubber," *Rubber Chem. Technol.*, vol. 66, no. 5, pp. 754–771, 1993.
[24] Y. Elsayed *et al.* "Finite element analysis and design optimization of a pneumatically actuating silicone module for robotic surgery applications," *Soft Robot.*, vol. 1, no. 4, pp. 255–262, 2014.
[25] D. N. Lee, "A theory of visual control of braking based on information about time-to-collision," *Perception*, vol. 5, no. 4, pp. 437–459, 1976.
[26] E. Baird, N. Boeddeker, M. R. Ibbotson, and M. V. Srinivasan, "A universal strategy for visually guided landing," in *Proc. Nat. Acad. Sci., USA*, vol. 110, no. 46, pp. 18 686–18 691, 2013.
[27] Z. Zhang, P. Xie, and O. Ma, "Bio-inspired trajectory generation for UAV perching," in *Proc. IEEE/ASME Int. Conf. Adv. Intell. Mechatronics*, 2013, pp. 997–1002.
[28] J. Redmon, S. Divvala, R. Girshick, and A. Farhadi, "You only look once: Unified, real-time object detection," in *Proc. IEEE Conf. Comput. Vis. Pattern Recognit.*, 2016, pp. 779–788.
[29] D. Gandhi, L. Pinto, and A. Gupta, "Learning to fly by crashing," arXiv preprint arXiv:1704.05588, 2017.
[30] A. Giusti *et al.*, "A machine learning approach to visual perception of forest trails for mobile robots," *IEEE Robot. Autom. Lett.*, vol. 1, no. 2, pp. 661–667, 2016.
[31] L. Bottou, "Large-scale machine learning with stochastic gradient descent," in *Proc. COMPSTAT*, Springer, 2010, pp. 177–186.
[32] Robot operating system (ROS), 2017. [Online]. Available: http://wiki.ros.org/

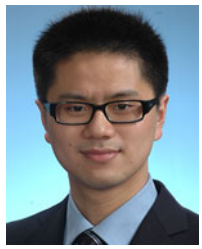

Cai Luo (SM'17) received the B.Eng. degree in electrical information engineering from Wuhan University, Wuhan, China, in 2006; the M.Sc. degree in electrical and electronic engineering from the University of Sheffield, Sheffield, U.K., in 2008; and the Ph.D. degree in electronic and computer engineering, robotics and telecommunication from the University of Genoa, Genoa, Italy, in 2012.

From 2012 to 2013, he was a Marie Curie Fellow in the Technical Research Centre of Finland (VTT), Finland. From 2013 to 2015, he was an Assistant Researcher in the Department of Automation, Tsinghua University, Beijing, China. He is currently a Lecturer in the China University of Petroleum (East China), Qingdao, China. His current research interests include unmanned aerial vehicle biomimetic design and dynamics and control of robotic systems.

Leijian Yu received the B.Eng. degree in electrical information engineering from China University of Petroleum (East China), Qingdao, China, in 2015. He is currently working toward the M.Eng. degree in the information and communication engineering from China University of Petroleum (East China).

His current research interests include machine learning with applications on unmanned aerial vehicles (UAV), UAV vision-based autonomous navigation, and 3-D reconstruction of an unknown environment.

Peng Ren (SM'16) received the B.Eng. and M.Eng. degrees, both in electronic engineering, from Harbin Institute of Technology, Harbin, China, and the Ph.D. degree in computer science from the University of York, York, U.K., YO10 5DD.

He is currently a Full Professor in the College of Information and Control Engineering, China University of Petroleum (East China), Qingdao, China. His major interests include remote sensing and machine learning. He has published more than 40 academic papers in these research fields.

Dr. Ren received the K. M. Scott prize from the University of York in 2011 and was a coauthor of the Eduardo Caianiello best student paper at the 18th International Conference on Image Analysis and Processing in 2015.